Int J Thermophys (2007) 31:42–54
DOI 10.1007/s10765-009-0691-2

Influence of Primary Milling on Structural and Electrical Properties of $Bi_4Ti_3O_{12}$ Ceramics Obtained by Sintering Process

J. Dercz · G. Dercz · K. Prusik · B. Solecka · A. Starczewska · J. Ilczuk

Received: 1 April 2009 / Accepted: 29 November 2009 / Published online: 19 December 2009

Abstract In this article, the influence of primary mechanical milling of precursors on the microstructure and dielectric properties of $Bi_4Ti_3O_{12}$ ceramics was studied. Precursor material (mixture of Bi_2O_3 and TiO_2 powders) was ground by a high-energy attritorial mill for (1, 3, 5, and 10) h. $Bi_4Ti_3O_{12}$ ceramics were obtained by a solid-state reaction process, synthesized at an intermediate temperature (800 °C) and finally sintered at high temperature (1140 °C). Structure studies were performed by X-ray diffraction (XRD) and scanning electron microscopy techniques. XRD patterns were analyzed by the Rietveld method using the DBWS 9807a program. The thermal properties of the studied materials were measured using differential thermal analysis and thermal gravimetric techniques. These studies indicate that one-, three-, and five-hour primary high-energy ball milling followed by sintering is a promising technique for pure $Bi_4Ti_3O_{12}$ ferroic ceramics preparation. The investigation of $Bi_4Ti_3O_{12}$ shows that ceramics obtained from a precursor and milled for 5 h have the best dielectric properties.

Keywords $Bi_4Ti_3O_{12}$ ceramics · Ferroelectric · High-energy ball milling · Rietveld method · Sintering · Thermal properties

J. Dercz · J. Ilczuk
Department of Material Science, University of Silesia, Żeromskiego 3, 41-200 Sosnowiec, Poland

G. Dercz (✉) · K. Prusik
Institute of Materials Science, University of Silesia, Bankowa 12, 40-007 Katowice, Poland
e-mail: grzegorz.dercz@us.edu.pl

B. Solecka · A. Starczewska
Institute of Physics, Silesian University of Technology, Krasińskiego 8, 40-007 Katowice, Poland

1 Introduction

Bismuth titanate $Bi_4Ti_3O_{12}$ (BIT) is a typical ferroelectric material belonging to the Aurivillius compounds family [1,2]. Its interesting electro-optic properties, low dielectric permittivity, high Curie temperature (675 °C), and large spontaneous polarization make it useful in the field of electro-optics and microelectronics as non-volatile ferroelectric random access memories (NV-FeRAM's) or high-temperature piezoelectric components [3–12].

The layer-perovskite materials described by Aurivillius are named after him as Aurivillius compounds [1,2]. The chemical formula of Aurivillius compounds is $(Bi_2O_2)^{2+}(A_{m-1}B_mO_{3m+1})^{2-}$, where A represents 12-fold coordinated cations with low valences in the perovskite sublattice (Ba^{2+}, Sr^{2+}, Ca^{2+}, Bi^{3+}, Pb^{4+}); B denotes the octahedral site with high valences (Fe^{3+}, Nb^{5+}, Ti^{4+}, Ta^{5+}, Mo^{6+}, W^{6+}, Mn^{2+}); and m is the number of octahedral layers in the perovskite-like layers between the bismuth-oxygen layers stacked along the c direction in the crystal structure. In the layer structure of $Bi_4Ti_3O_{12}$, the $(Bi_2Ti_3O_{10})^{2-}$ layers are sandwiched between two $(Bi_2O_2)^{2+}$ layers along its crystallographic c axis. Ti ions are enclosed by an oxygen octahedral, and are linked through corners forming O–Ti–O linear chains. Bi ions occupy the spaces in the framework of the TiO_6 octahedral.

Mechanical activation based on the milling process is recognized as a suitable technique for the synthesis of a wide range of advanced materials by mechanical alloying. Many complex, multicomponent metallic, and ceramic materials, which may be otherwise difficult to synthesize by conventional high temperature treatment, have been effectively prepared by high-energy ball milling (HEBM). In addition, intensive milling is an important means for preparation of nanocrystalline and amorphous materials, as well as for milling-induced self-sustaining reactions [13–18].

In recent years, some authors reported a method for preparation of ferroelectric $Bi_4Ti_3O_{12}$ compounds. They obtained it using mechanically synthesized precursors followed by sintering processes [19–26]. However, no information about the effect of manufacturing process data (such as a milling time) on compound structure and dielectric properties has been presented to date.

The aim of this study is an attempt at preparing $Bi_4Ti_3O_{12}$ ceramics by mechanical synthesis followed by two-stage free sintering processes. The influence of the processing parameters on the crystal microstructure, and dielectric and ferroelectric properties of $Bi_4Ti_3O_{12}$ ceramics are discussed.

2 Measurements

2.1 Specimens

The initial powders used in this study were commercially available bismuth oxide (Bi_2O_3, POCH, 99.8 %) and titanium oxide (TiO_2) in an anatase crystal form (POCH 99.9 % purity). The powders of simple oxides for the milling process were prepared according to the following formula: $2Bi_2O_3 + 3TiO_2 \rightarrow Bi_4Ti_3O_{12}$.

As-prepared powder was ground in an attritorial mill. The milling operation was carried out in a Fritsch Pulverisette 5 planetary HEBM system in an air atmosphere for (1, 3, 5, and 10) h. A 2 dm^3 stainless-steel chamber, and stainless-steel balls of 6 mm diameter, and 10:1 ball-to-powder weight ratio were used. The milling speed was set at 250 rpm.

After the milling process, the precursor powder was pressed to obtain disks of 10 mm in diameter. To produce the desired ceramics, two sets of the free sintering technique were applied. The first stage was conducted at 800 °C (synthesis) for 5 h, whereas the second one was carried out at 1140 °C (sintering process) for a duration of 5 h as well.

2.2 Procedures

The thermal behavior of milled powders was investigated from room temperature to 1000 °C using differential thermal analysis (DTA) and thermal gravimetric (TG) techniques.

X-ray diffraction data were collected using the X-Pert Philips diffractometer equipped with a curved graphite monochromator on a diffracted beam. It was supplied by a current intensity of 30 mA and voltage of 40 kV. The 1.54178 Å $Cu_{K\alpha}$ spectral line was used. The diffraction pattern was recorded by the "step-scanning" method in the 2θ range from 10° to 140° with 0.04° steps.

The structure of the studied samples has been calculated by a powerful Rietveld's whole X-ray profile fitting technique using the DBWS 9807a program [27]. The profile function used to adjust the calculated to the observed diffractograms was the pseudo-Voigt one [28]. The lattice parameters, atomic positions, and occupation factors of the calculated XRD pattern are adjusted to the observed value until a minimal deviation is reached [29,30]. The best-fitting curve obtained from the least-squares method assumes a minimal sum of squared deviations (least-squares error) from a given set of data. The mass fraction of each component was determined from the optimized scale factors using the relation proposed by Hill and Howard [31]. Moreover, Rietveld method was applied to qualitative phase composition verification.

The SEM (JEOL JSM-6480) and EDS techniques were used for the ceramic samples morphology analysis and their chemical composition, respectively.

A standard Sawyer-Tower circuit was used to obtain the polarization hysteresis (P–E) loop at 35 Hz, and an electric field of 420 $V \cdot cm^{-1}$ was applied to polarize the samples at 20 °C [32].

3 Results

Figure 1 shows an example of the XRD pattern of the powder mechanically activated by 1 h milling. Qualitative phase analysis of precursors in the samples milled for (1, 3, 5, and 10) h revealed the presence of Bi_2O_3 (ICDD PDF 71-2274), TiO_2 in anatas form (ICDD PDF 71-2274), and $Bi_2O_2CO_3$ (ICDD PDF 41-1488) phases. This carbonate phase was formed because Bi_2O_3 reacted with CO_2 in air. The $Bi_2O_2CO_3$ phase probably was formed only on the Bi_2O_3 fresh particle surfaces, and reduced

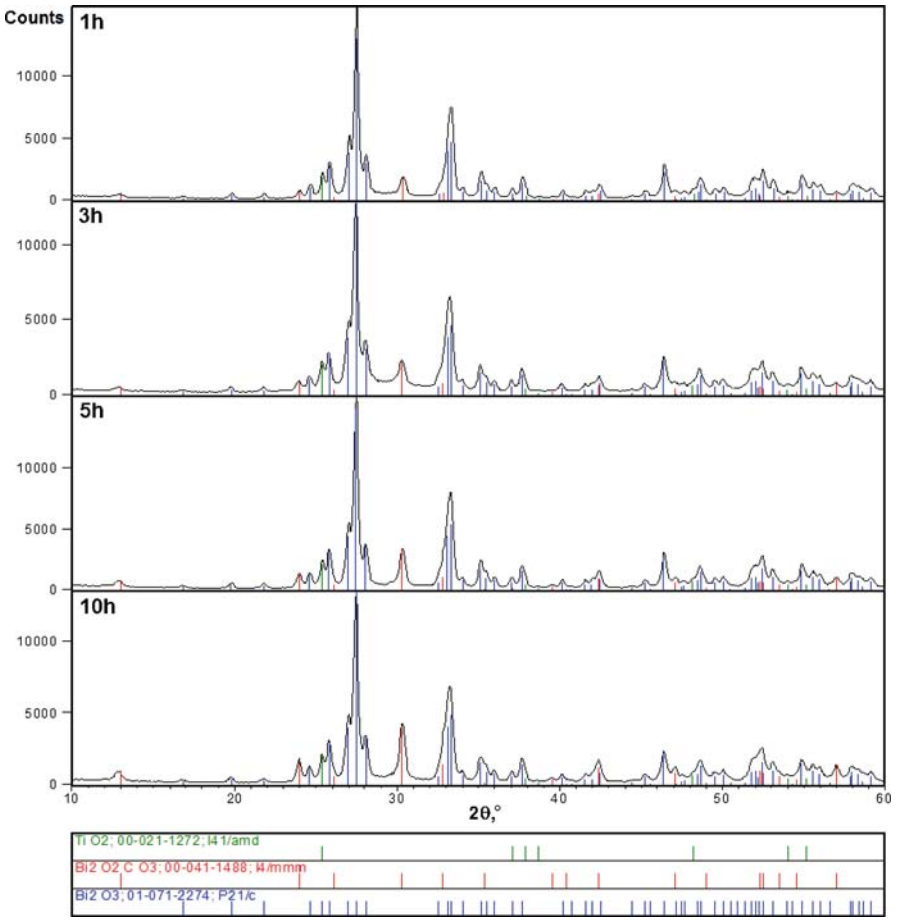

Fig. 1 X-ray diffraction patterns of precursor material mixture milled for (1, 3, 5, and 10) h

Table 1 Calculated contents for each phase in the samples milled for (1, 3, 5, and 10) h and as-prepared powder

Phase	Contents (mass%)				
	As-prepared	1 h	3 h	5 h	10 h
Bi_2O_3	79.5	71.9	68.1	65.6	62
$Bi_2O_2CO_3$	–	8.7	12.6	15.5	19.5
TiO_2	20.6	19.4	19.3	18.9	18.5

to a grain size during the HEBM process. Moreover, after mechanical activation the peaks were broadened and had lower intensities. This probably indicates decrease in the grain size and the formation of structural defects.

The calculated mass percent of each phase for the samples milled for (1, 3, 5, and 10) h is shown in Table 1. During the HEBM process, some changes in the contents of two bismuthal phases (Bi_2O_3 and $Bi_2O_2CO_3$) were observed.

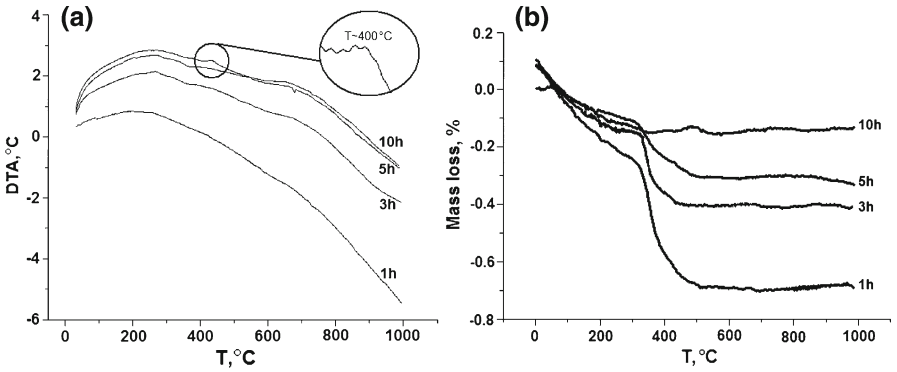

Fig. 2 **(a)** Differential scanning calorimetry (DSC) and **(b)** thermogravimetric (TG) curves of precursors in the samples milled for (1, 3, 5, and 10) h

After 1 h milling, the fractions of the Bi_2O_3 and $Bi_2O_2CO_3$ phases are equal to 71.9 mass% and 8.7 mass%, respectively. The longer the milling time (3, 5, and 10) h, the higher is the content of the carbonate phase. For 10-hour milled samples, its content reaches 19.5 mass%, while the bismuth oxide mass fraction decreases to 62.0 mass% (Table 1).

Figure 2a shows DTA heating cycles of powders milled for (1, 3, 5, and 10) h. Broadening of the exothermic peak observed at about 4000 °C for a 10-hour milled sample is attributed to the decomposition of a $Bi_2O_2CO_3$ phase, as is indicated by XRD measurement.

TG results for the milled powders are depicted in Fig. 2b. The precursor powder milled for 1 h exhibits an overall mass loss not exceeding 0.8 % at temperatures from 20 °C to 1000 °C. Finally for the 10-hour milled samples, the mass decrease is about 0.1 %

Figure 3 shows the SEM images of a sample milled for 1 h and 10 h. The images reveal that the specimens consist of fine-grained spherical and fibrous particles. The increase of fibrous grain content with an increase of the milling time is observed. The images indicate a rather loose, skeleton-type structure. Moreover, the strong agglomeration of powders can be noticed (Fig. 3c).

Figure 4 shows the XRD patterns of the BIT samples after the sintering process using the mixture of precursor oxides milled for 1 h and 10 h (marked as BIT 1 h, BIT 10 h, respectively), whereas Fig. 6 presents Rietveld refinement plot phase analysis for a precursor milled for 10 h (marked as BIT 10h). XRD investigations of the samples BIT 1 h, BIT 3 h, and BIT 5 h enabled the identification of only one crystalline phase— $Bi_4Ti_3O_{12}$ (ICDD PDF 35-0795). Qualitative phase analysis of a BIT 10 h sample shows the presence of two phases: $Bi_4Ti_3O_{12}$ (ICDD PDF 35-0795) and $Bi_{20}TiO_{32}$ (ICDD PDF 42-0202) (Fig. 4). The $Bi_4Ti_3O_{12}$ phase is the main component of the BIT 10h sample (98.3 mass%). On the other hand, the content of the $Bi_{20}TiO_{32}$ phase is much lower (1.7 mass%) (Table 2). The $Bi_{20}TiO_{32}$ phase is an intermediate phase in the formation of $Bi_4Ti_3O_{12}$. Chemical analysis revealed that BIT ceramics contained small contamination (Fe $\sim$ 0.1 mass%). Authors suppose that the presence

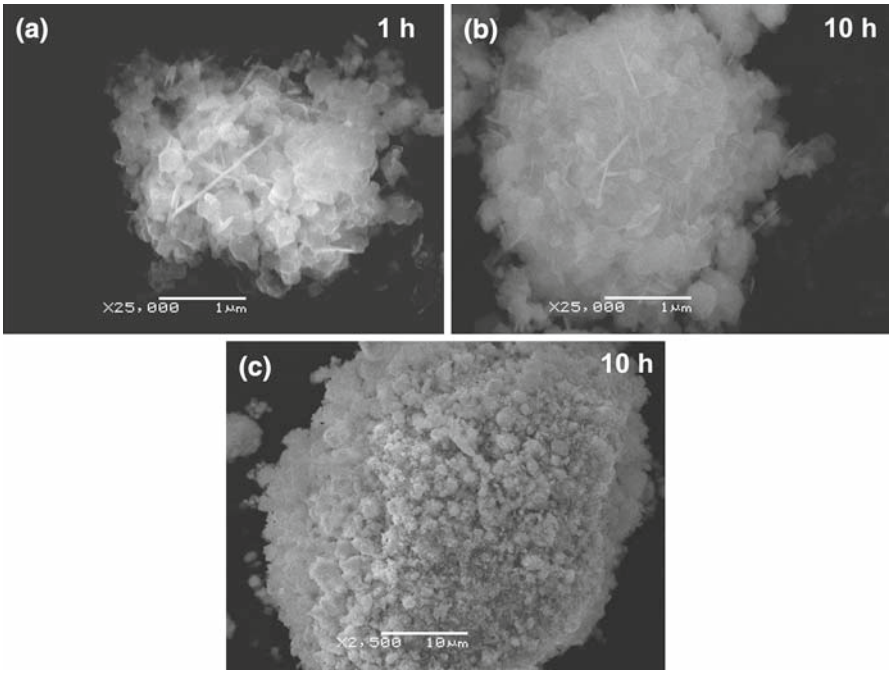

Fig. 3 SEM images of ground sample for **(a)** 1 h and **(b, c)** 10 h

of the $Bi_{20}TiO_{32}$ phase in the ceramics is connected with agglomerate formation during the milling process (Fig. 3c). Results of the qualitative and quantitative EDS analyses of the BIT 10h ceramic are shown in Fig. 5.

In this study, the Rietveld refinement technique was used to investigate the changes of crystal structure of the BIT samples obtained from sintering processes performed on the previously milled samples (Table 1). An example of a Rietveld output pattern obtained after the free sintering process of samples milled previously for 5 h is presented in Fig. 6. The values of fitting parameters (Table 2): R_{wp}, R_{exp}, and goodness-of-fit S obtained for powder and composite samples are in the range of: $R_{wp} = 7.29\,\%$ to $7.83\,\%$, $R_{exp} = 5.10\,\%$ to $5.22\,\%$, and S (goodness-of-fit) = 1.43 to 1.50 (Table 2).

The values of the lattice parameters (a_0, b_0, and c_0) for all concerned phases determined by Rietveld method are given in Table 2. The uncertainty in the lattice parameter determination found using an alumina plate SRM 1976 standard is 0.015 % based on ICDD files. As a starting structural model for Rietveld analysis, the orthorhombic perovskite-type (No. 65) structure with unit cell parameters: $a_0 = 0.54489$ nm, $b_0 = 3.2815$ nm, and $c_0 = 0.54100$ nm was used [32]. Those parameters correspond with the standard data for $Bi_4Ti_3O_{12}$ (ICDD card 35-0795) phase. Comparisons of the calculated lattice parameters for BIT samples and literature values show that the primary milling process causes $Bi_4Ti_3O_{12}$ unit cell deformation. The lowest values of lattice parameters and the volume elementary cell (Table 2) were obtained for the BIT 5h sample after a 5 h milling process of substrates.

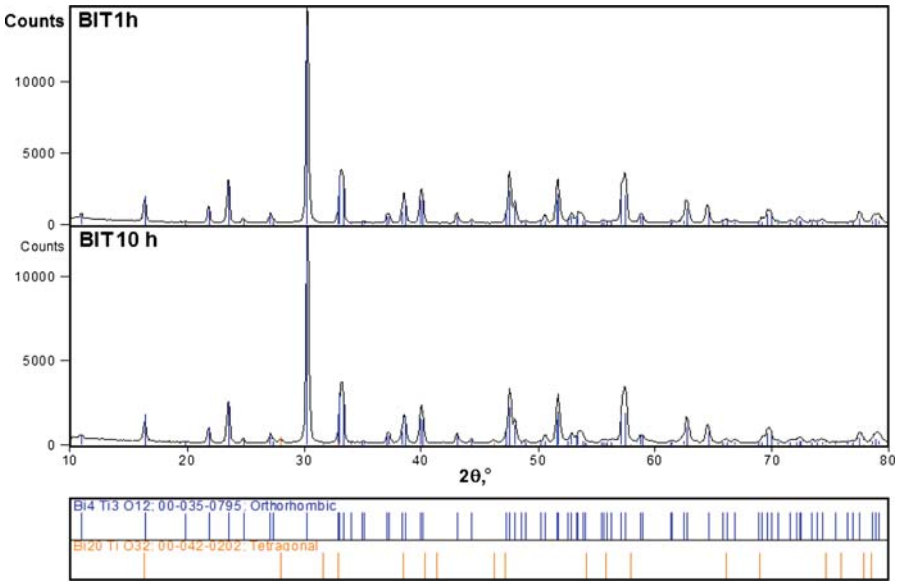

Fig. 4 X-ray diffraction patterns of ceramics obtained after free sintering process of samples milled previously for (1 (BIT 1 h) and 10 (BIT 10 h)) h

Table 2 Lattice parameters, phase contents, and fitting parameters calculated by Rietveld for BIT ceramics

Sample	Phase	Lattice parameters (nm)			Phase contents (mass%)	Fitting parameters		
		a_0	b_0	c_0		R_{wp} (%)	R_{exp} (%)	S
BIT 1 h	$Bi_4Ti_3O_{12}$	0.54417(4)	3.2827(3)	0.54108(5)	100	7.29	5.10	1.43
BIT 3 h	$Bi_4Ti_3O_{12}$	0.54411(4)	3.2822(3)	0.54112(5)	100	7.56	5.18	1.46
BIT 5 h	$Bi_4Ti_3O_{12}$	0.54477(4)	3.2816(3)	0.54104(5)	100	7.73	5.22	1.50
BIT 10 h	$Bi_4Ti_3O_{12}$	0.54427(4)	3.2826(3)	0.54111(5)	98.3	7.83	5.12	1.49
	$Bi_{20}TiO_{32}$	1.0153(1)	1.0153(1)	1.0153(1)	1.7			

Generally the $Bi_4Ti_3O_{12}$ lattice parameters determined by Rietveld method and those taken directly from ICDD files are in good agreement. Small difference between lattice parameters can be the result of fine non-stoichiometry of phases.

Figure 7 shows the SEM images of fractured BIT ceramics prepared by the sintering method of previously milled precursors. The images exhibit plate-like grains, overlapping one another. Such morphology is characteristic for layer structures of the Aurivillius type. The average thickness of lamella is about 0.5 μm to 2 μm and increases with the milling time. The same kind of grain orientation was found in ceramics obtained from precursor powder milled for 5 h (BIT 5 h—Fig. 7). The morphology for other samples (BIT 1 h, BIT 3 h, and BIT 10 h) shows grains of different orientations (Fig. 7). Moreover, the SEM study revealed that the BIT 10h sample has the largest, spherical-like, and plate-like grains (Fig. 7—BIT 10 h). Probably the

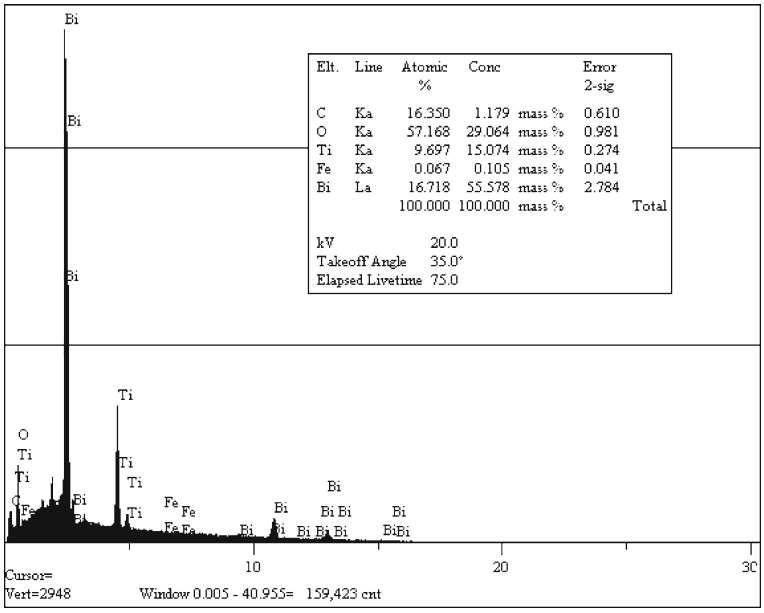

Fig. 5 EDS analysis of BIT 10h sample

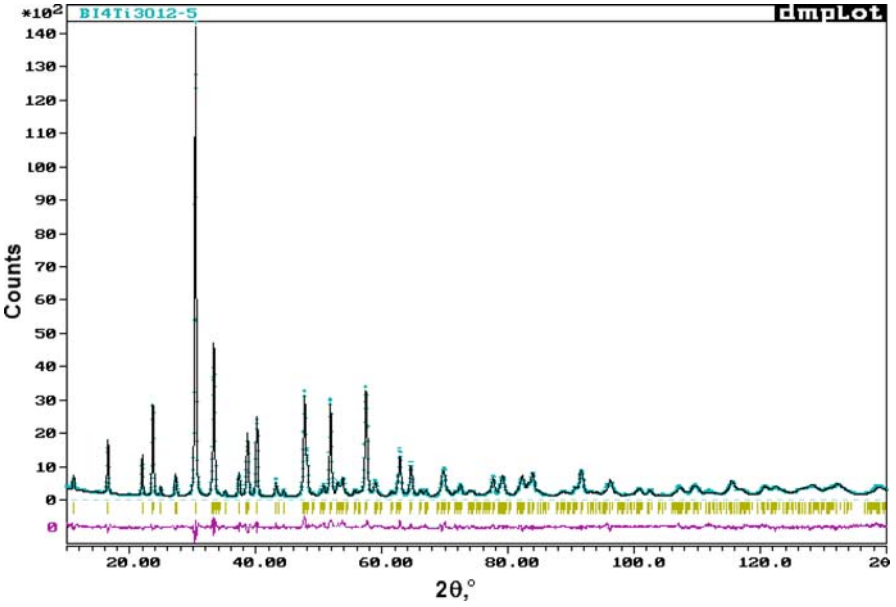

Fig. 6 Rietveld output of X-ray diffraction pattern obtained after free sintering process of samples milled previously for 5 h

presence of the $Bi_{20}TiO_{32}$ phase causes the increase in grain size when the milling time increases to 10 h. This phase is a liquid at high temperature and could be liable for the increase of grain size.

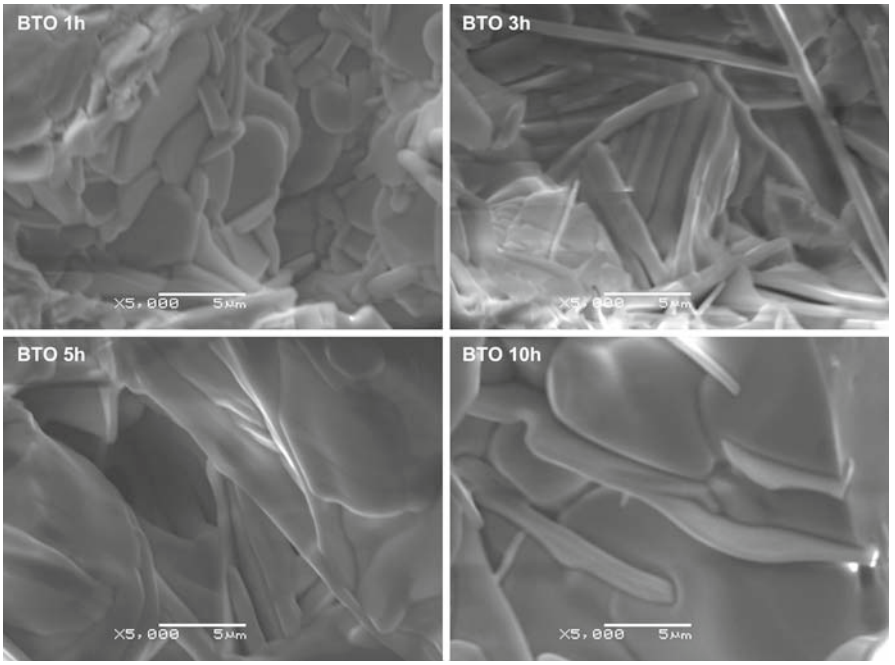

Fig. 7 Fractures of $Bi_4Ti_3O_{12}$ ceramics obtained by the sintering process of samples milled previously for (1 (BIT 1 h), 3 (BIT 3 h), 5 (BIT 5 h), and 10 (BIT 10 h))h

Table 3 Experimental (ρ_{exp}), theoretical (ρ_{theor}) density, and parameters (E_c, P_r, and P_s) of polarization-electric hysteresis loops (P–E) of the BIT samples at $U = 120$ V and 60 V

Sample	Density (ρ)		E_c ($V \cdot cm^{-1}$)	P_r ($\mu C \cdot cm^{-2}$)	P_s ($\mu C \cdot cm^{-2}$)	E_c ($V \cdot cm^{-1}$)	P_r ($\mu C \cdot cm^{-2}$)	P_s ($\mu C \cdot cm^{-2}$)
	ρ_{exp} $g \cdot cm^{-3}$	ρ_{exp}/ρ_{theor} (%)	$U = 120$ V			$U = 60$ V		
BIT 1 h	7.67	95.4	1013	0.012	0.020	472	0.006	0.013
BIT 3 h	7.76	96.5	1005	0.015	0.030	523	0.008	0.015
BIT 5 h	7.92	98.5	999	0.014	0.031	520	0.007	0.015
BIT 10 h	7.87	97.9	1156	0.015	0.026	468	0.007	0.014

Experimental and theoretical densities are given in Table 3. The BIT 5h specimen showed the highest relative density, which is 98.5 % of the theoretical density ($8.04\ g \cdot cm^{-3}$), compared to the other BIT samples (Table 3). When the milling time of precursors was increased to 10 h, the experimental relative density slightly decreased to 97.9 % (Table 3). This is the result of an increase in the grain size and the presence of the $Bi_{20}TiO_{32}$ phase.

The ferroelectric properties of the BIT samples were investigated using a Sawyer–Tower circuit and monitored using a digitizing oscilloscope. Figure 8 shows the polarization hysteresis loops (P–E) measured at 35 Hz for $Bi_4Ti_3O_{12}$ ceramics

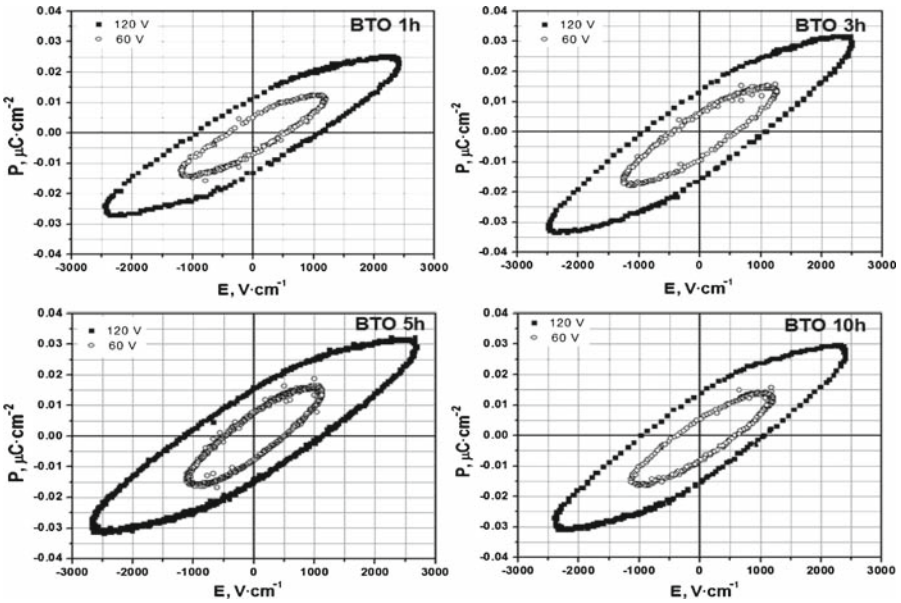

Fig. 8 Polarization–electric field hysteresis loops for the BIT 1h, BIT 3h, BIT 5h, and BIT 10h samples measured at an applied electric field of $120\,\mathrm{V}\cdot\mathrm{cm}^{-1}$ and $60\,\mathrm{V}\cdot\mathrm{cm}^{-1}$ at 35 Hz

after the sintering process at 1140 °C of precursor powder milled for 1 h (BIT 1 h), 3 h (BIT 3 h), 5 h (BIT 5 h), and 10 h (BIT 10 h). Maximum spontaneous polarization (P_s) was obtained for sample BTF 5 h. It is equal to $0.031\,\mu\mathrm{C}\cdot\mathrm{cm}^{-2}$ and $0.015\,\mu\mathrm{C}\cdot\mathrm{cm}^{-2}$ at $120\,\mathrm{V}\cdot\mathrm{cm}^{-1}$ and $60\,\mathrm{V}\cdot\mathrm{cm}^{-1}$, respectively. Similar values of spontaneous polarization were calculated for the BIT 3h sample. In addition, the BIT 5h sample exhibits the highest remanent polarization (P_r) of $0.014\,\mu\mathrm{C}\cdot\mathrm{cm}^{-2}$ and $0.007\,\mu\mathrm{C}\cdot\mathrm{cm}^{-2}$ at $120\,\mathrm{V}\cdot\mathrm{cm}^{-1}$ and $60\,\mathrm{V}\cdot\mathrm{cm}^{-1}$, respectively. The BIT 3h sample shows a coercive field $E_c = 1005\,\mathrm{V}\cdot\mathrm{cm}^{-1}$, while BIT 5 h shows the lowest value of $E_c = 999\,\mathrm{V}\cdot\mathrm{cm}^{-1}$ (Table 3). When the milling time of precursors increases from 5 h to 10 h, E_c of the BIT 10h sample increases up to $1156\,\mathrm{V}\cdot\mathrm{cm}^{-1}$. The shape of polarization loops for all samples is slightly different and is far from rectangular, suggesting that spontaneous polarization should be much larger if the applied driven field has a higher value. The very large coercive field indicates that the switching of polarization is more difficult in the BIT samples, due to the pinning effect caused by various defects inside. Moreover, the polarization hysteresis loops from BIT samples were not really saturated. Probably, the grain density affects the profile of the hysteresis loops and polarization parameters.

Figure 9 shows the temperature dependence of dielectric constants (ε) and dielectric loss ($\tan\delta$) of the BIT samples measured at 1 MHz. For the BIT 1h, BIT 3h, BIT 5h, and BIT 10h samples, the Curie temperature was observed at 675 °C.

The dielectric peak for the BIT 5h sample has the smallest width. For the BIT 10h sample, broadening of the peak was observed (Fig. 9a). Moreover, for the BIT 1h sample an additional peak (at about 450 °C to 500 °C) appeared. The anomalous behavior

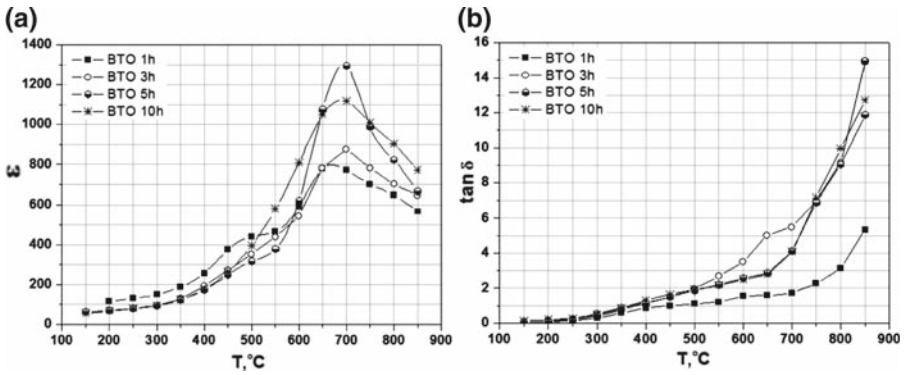

Fig. 9 Dielectric constant and dielectric loss of the BIT 1h, BIT 3h, BIT 5h, and BIT 10h samples as a function of temperature

of BIT near 450 °C to 500 °C is connected with the spontaneous dipole re-orientation and point defect relaxation (local ionic jumps) such as oxygen vacancies [33,34].

Figure 9a depicts that $Bi_4Ti_3O_{12}$ ceramics show a ferroelectric characteristic rather than a relaxor characteristic because the dielectric constant decreases when the sample temperature is higher than the Curie temperature. Moreover, dielectric peak broadening, observed for the all samples, is connected with oxygen-vacancy-related dielectric relaxation [35,36]. Furthermore, an increase of the milling time of precursors from 1 h to 5 h at first causes an increase of the dielectric constant up to 1293, but after 10 h of milling time, ε decreases to 1117 (Table 4). This is the effect of a decrease of the fraction of pores and an increase of the grain size. Figure 9b also shows that the dielectric loss grows with increasing temperature. The dielectric loss values of BIT 1h and BIT 3h ceramics critically increase from 0.015 to 0.05 as the milling time of precursors increases from 1 h to 3 h. For the other samples (BIT 5 h and BIT 10 h), tanδ values are the same and equal to 4.1 %. Generally, the dielectric loss valley corresponds to the dielectric permittivity peak. Jardiel et al. [37] explained the relationship between the conductivity and the aspect ratio of the platelets in Aurivillius phases [37]. They indicated that the conductivity in BIT decreases when the aspect ratio (length/thickness) of the grains decreases. This behavior in dielectric losses has been attributed to different phenomena.

The ionic conductivity is connected with the presence of the oxygen vacancies and takes place predominantly in the *ab* plane. On the other hand, the electronic conductivity (*p*-type) occurs along the *c* axis [38,39].

Because each orientation has a predominant charge transport mechanism, the average activation energy changes with the aspect ratio of the plate-like grains [37].

Table 4 Curie temperature (T_c), dielectric constant (ε), and dielectric loss (tanδ) of BIT samples at 1 MHz

	BIT 1 h	BIT 3 h	BIT 5 h	BIT 10 h
T_{CE} (°C)	675			
ε at T_{CE}	800	876	1293	1117
tanδ (%) at T_{CE}	1.5	5.0	4.1	4.1

4 Conclusions

The influences of the processing parameters on the crystal microstructure, and dielectric and ferroelectric properties of $Bi_4Ti_3O_{12}$ ceramics were investigated in this study. XRD analysis showed that HEBM for (1, 3, and 5) h followed by sintering can be used to obtain single-phase ferroic $Bi_4Ti_3O_{12}$ ceramics. Sintering processes of precursors milled longer than 5 h lead to formation of multiphase ceramics. Moreover, SEM observation of morphology reveals a classical plate-like form, typically observed in $Bi_4Ti_3O_{12}$ ceramics. The BIT 5h sample reveals the highest experimental density. The best ferroelectric properties were observed for well-sintered BIT 5h ceramics. Maximum spontaneous polarization (P_s) and highest dielectric constants (ε) were obtained for sample BTF 5 h, and P_s is equal to $0.031\ \mu C \cdot cm^{-2}$ at $120\ V \cdot cm^{-1}$ and 1293 °C.

In conclusion, it was found that the optimal milling time of precursor oxide powders for carrying out the sintering process is equal to 5 h. The obtained ceramics then contain one phase and exhibit the best electrical properties for practical applications.

Acknowledgment The substrates for synthesis are financially supported by Polish Committee for Scientific Research (Grant N507 142 31/3568).

References

1. B. Aurivillius, Arkiv. Kemi **1**, 499 (1949)
2. T. Kikuchi, A. Watanabe, K. Uchida, Mater. Res. Bull. **12**, 299 (1977)
3. B.H. Park, B.S. Kang, S.D. Bu, T.W. Noh, J. Lee, W. Joe, Nature **401**, 682 (1999)
4. U. Chon, H.M. Jang, M.G. Kim, C.H. Chang, Phys. Rev. Lett. **89**, 87601 (2002)
5. J.G. Lisoni, P. Millán, E. Vila, J.L.M. De Vidales, T. Hoffmann, A. Castro, Chem. Mater. **13**, 2084 (2001)
6. J. Ricote, L. Pardo, A. Castro, P. Millán, J. Solid State Chem. **160**, 54 (2001)
7. L.B. Kong, J. Ma, W. Zhu, O.K. Tan, Mater. Lett. **51**, 108 (2001)
8. P. Millán, J.M. Rojo, L. Pardo, J. Ricote, A. Castro, Mater. Res. Bull. **36**, 1277 (2001)
9. I.F. Vasconcelos, M.A. Pimenta, A.S.B. Sombra, J. Mater. Sci. **36**, 587 (2001)
10. S.H. Ng, J. Xue, J. Wang , J. Am. Ceram. Soc. **85**, 2660 (2002)
11. T. Kojima, T. Watanabe, H. Funakubo, K. Saito, M. Osada, M. Kakihana, J. Appl. Phys. **93**, 1707 (2003)
12. Y. Kan, J. Xihai, P. Wang, Y. Li, Y.-B. Chen, D. Yan, Mater. Res. Bull. **38**, 567 (2003)
13. C. Suryanarayana, Prog. Mater. Sci. **46**, 1 (2001)
14. C.C. Koch, Ann. Rev. Mater. Sci **19**, 121 (1989)
15. L. Schultz, J. Less-Common Met. **145**, 233 (1988)
16. A.W. Weeber, H. Bakker, Physica. B **153**, 93 (1988)
17. C.C. Koch, Nanostruct. Mater **2**, 109 (1993)
18. A.R. Yavari, Mater. Trans. JIM **36**, 228 (1995)
19. J. Wang, J.M. Xue, D.M. Wan, B.K. Gan, J. Solid State Chem. **154**, 321 (2000)
20. L.B. Kong, J. Ma, W. Zhu, O.K. Tan , Mater. Lett. **51**, 108 (2001)
21. B.D. Stojanovic, A.Z. Simoes, C.O. Paiva-Santos, C. Quinelato, E. Longo, J.A. Varela, Ceram. Int. **32**, 707 (2006)
22. B.D. Stojanovic, C.O. Paiva-Santos, C. Jovalekic, A.Z. Simoes, M. Filho, Z. Lazarevic, J.A. Varela, Mater. Chem. Phys. **96**, 471 (2006)
23. C.H. Yau, R. Palan, K. Tran, R.C. Buchanan, Appl. Phys. Lett. **85**(20), 4714 (2004)
24. Y.L. Du, G. Chan, M.S. Zhang, Solid State Commun. **132**, 175 (2004)
25. F. Zhang, T. Karaki, M. Adachi, Jpn. J. Appl. Phys. **45**(9B), 7385 (2006)
26. B.D. Stojanovic, C.O. Paiva-Santos, M. Cilense, C. Jovalekic, Z.Z Lazarevic, Mater. Res. Bull. **43**, 1743 (2008)

27. H.M. Rietveld, J. Appl. Cryst. **3**, 65 (1969)
28. R.A. Young, D.B. Wiles, Adv. X-ray Anal. **1** (1980)
29. R.A. Young, in *The Rietveld Method* (Oxford University Press, Oxford, 1993), pp. 17–32
30. R. Bouregba, G. Poullain, J. Appl. Phys. **93**, 522 (2003)
31. R.J. Hill, C.J. Howard, J. Appl. Cryst. **20**, 467 (1987)
32. J.F. Dorrian, R.E. Newnham, D.K. Smith, M.I. Kay, Ferroelectrics **3**, 17 (1971)
33. H.S. Shulman, D. Damjanovic, N. Setter, J. Am. Ceram. Soc. **83**, 528 (2000)
34. B. Jimenez, R. Jimenez, A. Castro, P. Millán, L. Pardo, J. Phys.-Condens. Mater. **13**, 7315 (2001)
35. Y. Wu, M.J. Forbess, S. Seraji, S.J. Limmer, T.P. Chou, G.Z. Cao, J. Appl. Phys. **89**, 5647 (2001)
36. W. Li, K. Chen, Y.Y. Yao, J.S. Zhu, Y.N. Wang, Appl. Phys. Lett. **85**, 4717 (2004)
37. T. Jardiel, A.C. Caballero, M. Villegas, J. Eur. Ceram. Soc. **27**, 4115 (2007)
38. M. Takahashi, Y. Noguchi, M. Miyayama, Jpn. J. Appl. Phys. **41**, 7053 (2002)
39. M. Takahashi, Y. Noguchi, M. Miyayama, Jpn. J. Appl. Phys. **42**, 6222 (2003)